mater.scichina.com link.springer.com

Published online 18 February 2022 | https://doi.org/10.1007/s40843-021-1935-5
Sci China Mater 2022, 65(6): 1485–1494

Tailoring $Sr_2Fe_{1.5}Mo_{0.5}O_{6-\delta}$ with Sc as a new single-phase cathode for proton-conducting solid oxide fuel cells

Liling Zhang[†], Yanru Yin[†], Yangsen Xu, Shoufu Yu and Lei Bi[*]

ABSTRACT **Sc-doped $Sr_2Fe_{1.5}Mo_{0.5}O_{6-\delta}$ (SFMSc) was successfully synthesized by partially substituting Mo in $Sr_2Fe_{1.5}Mo_{0.5}O_{6-\delta}$ (SFM) with Sc, resulting in a higher proton diffusion rate in the resultant SFMSc sample. Theoretical calculations showed that doping Sc into SFM lowered the oxygen vacancy formation energy, reduced the energy barrier for proton migration in the oxide, and increased the catalytic activity for oxygen reduction reaction. Next, a proton-conducting solid oxide fuel cell (H-SOFC) with a single-phase SFMSc cathode demonstrated significantly higher cell performance than that of cell based on an Sc-free SFM cathode, achieving 1258 mW cm^{-2} at 700°C. The performance also outperformed that of many other H-SOFCs based on single-phase cobalt-free cathodes. Furthermore, no trade-off between fuel cell performance and material stability was observed. The SFMSc material demonstrated good stability in both the CO_2-containing atmosphere and the fuel cell application. The combination of high performance and outstanding stability suggests that SFMSc is an excellent cathode material for H-SOFCs.**

Keywords: $Sr_2Fe_{1.5}Mo_{0.5}O_{6-\delta}$, cathode, single-phase, proton-conducting oxides, solid oxide fuel cells

INTRODUCTION

The solid oxide fuel cell (SOFC) could efficiently convert chemical energy into electricity while emitting little pollution, making it a viable technology for addressing the present environmental issue [1]. Although conventional SOFCs with oxygen-conducting electrolytes are commercially employed, the high working temperatures of traditional SOFCs (over 800°C) cause a number of issues, including reduced cell lifespan, challenges in selecting appropriate materials, and interlayer diffusions [2,3]. As a result, developing SOFCs that operate at lower temperatures (such as 700°C) is extremely desirable [4,5]. The development of highly conductive electrolyte materials and cathode materials with good catalytic activity at intermediate temperatures is required to reduce the SOFC working temperature [6,7]. In terms of electrolyte materials, proton-conducting oxides have been proposed as electrolytes for SOFCs in recent decades due to their high ionic conductivity at 600°C [8–10]. Furthermore, proton-conducting SOFCs (H-SOFCs) generate H_2O at the cathode side and so avoid fuel diffusion, demonstrating an advantage over SOFCs using oxygen-ion conducting electrolytes [11]. As a result, H-SOFC has been a hot topic in the the past decade [12–15].

Although highly conductive proton-conducting oxides as electrolytes can solve the intermediate temperature operation of SOFCs from an electrolyte perspective, the reduced working temperatures also result in sluggish cathode activities, resulting in high cathode polarization resistances and poor cell performance [16]. Traditional H-SOFC cathodes are derived from oxygen-ion conducting SOFCs. Despite the established satisfactory performance, the lack of proton-conduction in conventional cathode materials restricts the cathode reaction area and limits fuel cell performance [17,18]. Recently, it has been proposed to tailor cathode materials with protonation ability, which increases the cathode reaction sites and hence greatly enhances fuel cell efficiency [19,20]. A number of materials have been reported to exhibit protonation and improved cell performance [21–23], with the majority of these compounds based on perovskite materials containing cobalt [20,24]. The perovskite structure material incorporates H_2O for protonation [25], and cobalt plays an essential role in cathode catalytic activity [26,27]. However, issues such as cobalt evaporation at high temperatures and thermal mismatch between the cobalt-containing cathode and the electrolyte [28,29] have not been adequately addressed till now. As a result, the development of high-performance cathodes free of cobalt is of interest to many researchers.

$Sr_2Fe_{1.5}Mo_{0.5}O_{6-\delta}$ (SFM) is a well-investigated electrode for SOFCs because of its strong redox-ability [30], and it is frequently employed as the anode material rather than the cathode material for SOFCs because of its good catalytic activity under low oxygen partial pressure conditions [31–33]. Although various studies suggest that SFM may be utilized as the cathode for SOFCs [34,35], it is ineffective when compared with some other conventional perovskite materials. SFM has not been used for H-SOFCs for a long time due to its poor performance. Ren *et al.* [36] recently discovered that doping SFM with a small amount of Zr ions can adjust the oxygen vacancy in the oxide, hence promoting proton transport in the material. When compared with the Zr-doping technique, synthesizing SFM with a lower valence element may have a significant impact on the electrode performance. The substitution of Mo^{6+} with a lower valence element could result in more oxygen vacancies, thereby improving the cathode performance in H-SOFCs. The formation of oxygen vacancies can be represented in the following equation (using a 3+ element as an example): $A_2O_3 \xrightarrow{MoO_3} 2A'''_{Mo} + 3V^{\bullet\bullet}$. As

School of Resource Environment and Safety Engineering, University of South China, Hengyang 421001, China
[†] These authors contributed equally to this work.
[*] Corresponding author (email: lei.bi@usc.edu.cn or bilei81@gmail.com)

a result, we propose a novel cathode material, $Sr_2Fe_{1.5}Mo_{0.25}Sc_{0.25}O_{6-\delta}$ (SFMSc), in which Mo is largely replaced by Sc. The effect of Sc-doping was studied using both experimental and first-principles computations. The fuel cell devices with SFMSc as the cathode possess improved H-SOFCs performance.

EXPERIMENTAL SECTION

A standard combustion process was used to synthesize SFM, and SFMSc powders [37]. X-ray diffraction (XRD) was used to investigate the phase purity of SFM and SFMSc. X-ray photoelectron spectroscopy (XPS) was then used to characterize the chemical states of SFM and SFMSc. The chemical stability of SFMSc was investigated using *in-situ* high-temperature XRD, which involved heating the sample to high temperatures in a flow system with 10% CO_2 (balanced with air) at a rate of 50 mL min^{-1} and recording the XRD patterns of the sample at a specified temperature. Scanning transmission electron microscopy (STEM, JEM-2100F) was used to study the composition of the SFMSc. The electrical conductivity relaxation (ECR) tests were performed on dense SFM and SFMSc bars. The four-probe method was utilized to characterize the conductivity and time for SFM and SFMSc bars to reach equilibrium when the gas was changed from dry to wet (3% H_2O) air.

Theoretical calculations were carried out by the density functional theory (DFT) method using the Vienna *ab initio* simulation package [38]. The 2 × 2 × 2 supercell was used for the calculations of both SFM and SFMSc according to the literature [24,39]. The capacity of SFM and SFMSc to perform oxygen reduction reactions (ORR) was investigated by adsorbing an O_2 molecule on the surfaces of SFM and SFMSc and estimating the O_2 adsorption energy. For the surface calculation, the thickness of the vacuum layer was set to 15 Å. The climbing image nudged elastic band (CI-NEB) method [40] was used to calculate the dissociation energy.

Anode-supported $BaCe_{0.7}Zr_{0.1}Y_{0.2}O_{3-\delta}$ (BCZY) half-cells were fabricated using NiO-BCZY composite anode and BCZY electrolyte [37] and co-sintered at 1300°C for 6 h to evaluate the performance of SFM and SFMSc as cathodes for H-SOFCs. The SFM/SFMSc was deposited on the surface of the BCZY membrane before co-sintering the cathode layer with the half-cell at 850°C for 10 min in a microwave sintering furnace, resulting in complete cells. It is reported that the microwave sintering approach may adhere the cathode layer to the electrolyte at lower temperatures than the traditional sintering method, which mitigates potential interfacial reactions and preserves the cathode's ideal microstructure [41]. It should be emphasized that the cathode is only SFM or SFMSc without any electrolyte powder coupling. Wet H_2 was used as the fuel, while static air was used as the oxidant in the single cells. In the fuel cell test, the flow rate of H_2 fuel was 40 mL min^{-1}. An electrochemical workstation was used to record the cells' electrochemical performance (Squidstat Plus). The frequency range for the alternating current (AC) impedance test was set from 1 MHz to 0.1 Hz. Scanning electron microscopy (SEM) was used to examine the morphologies of the tested SFM and SFMSc cells.

RESULTS AND DISCUSSION

The XRD patterns of the synthesized SFM and SFMSc materials are shown in Fig. 1a, suggesting that both materials are pure phases. The magnified area view in Fig. 1b shows a peak shift to higher angles due to the incorporation of Sc into SFM, implying a smaller lattice volume for SFM after Sc-doping. The contraction of the lattice is also detected using a high-resolution transmission electron microscope (HRTEM), as shown in Fig. 1c, d. SFM and SFMSc have *d*-spacing values of 2.79 and 2.75 Å, respectively. The HRTEM results reveal that Sc-doping causes a contraction in the SFM lattice volume, which is consistent with the XRD analysis. However, the ionic radius of Sc^{3+} is 74.5 pm, which is larger than that of Mo^{5+} (61 pm) and Mo^{6+} (59 pm). In theory, replacing Mo with Sc should result in an expansion rather than a shrinkage of the lattice volume. As a result, various factors can be thought to influence the lattice volume. In the SFMSc lattice, the lower valence Sc^{3+} substitutes $Mo^{5+/6+}$. To compensate for the charge loss, the valence of Fe ions in the lattice may fluctuate in addition to the formation of extra oxygen vacancies. Fe^{3+} has a smaller ionic radius than Fe^{2+}, which could cause the lattice to shrink. The electrical structure of SFM and SFMSc elements was revealed using XPS investigation. Fig. 1e, f indicate that Fe^{2+} and Fe^{3+} can be detected; however, the concentration of Fe^{2+} and Fe^{3+} varies in SFM and SFMSc. The Fe^{2+}/Fe^{3+} ratio in SFM is 0.76, while it is 0.57 in SFMSc, indicating an increase in Fe^{3+} concentration following Sc-doping and confirming the hypothesis made above. The composition of SFMSc was confirmed further by STEM mapping, as shown in Fig. 1g, which shows an even distribution of each element with no discernible elemental segregations.

Aside from the effective fabrication of the SFMSc material, its chemical stability should also be investigated. The chemical stability of SFMSc was tested by exposing the powder to a CO_2-containing environment (10% CO_2 balanced with air) under various testing scenarios. The time evolution of the *in-situ* high-temperature XRD pattern of the SFMSc powder treated in the CO_2-containing atmosphere at 700°C is shown in Fig. 2a. Even under CO_2-containing conditions, there is no secondary phase formation as a function of operation duration, and the SFMSc phase remains stable after 10-h testing. Furthermore, the measurement was performed to investigate the phase stability of the SFMSc material at temperatures ranging from 100 to 800°C in a flowing CO_2 atmosphere. Fig. 2b demonstrates that the structure of SFMSc remains constant across the whole testing temperature range in a CO_2-containing environment. All the evidences suggest that SFMSc has strong chemical stability against CO_2, and therefore CO_2 corrosion to SFMSc should not be a serious issue. To obtain insight into the good stability of SFMSc against CO_2, the interaction between CO_2 and SFMSc was studied using DFT computations. The computation was carried out by adsorbing a CO_2 molecule on the surface of SFMSc, and there are two sites for the possible CO_2 adsorption, as shown in Fig. 2c. The CO_2 adsorption energy (E_{ads}) was computed using the equation: $E_{ads}=E_{surface+CO_2}-E_{surface}-E_{CO_2}$ [42], where the values are 0.68 eV for CO_2 adsorption on the Fe-O-Mo site and −1.28 eV for CO_2 adsorption on the Fe-O-Fe site, respectively. The positive value for the CO_2 adsorption energy indicates that CO_2 adsorption on the surface of SFMSc is unlikely at the Fe-O-Mo site. The negative value for the Fe-O-Fe site, on the other hand, indicates that CO_2 adsorption is thermodynamically favorable at this site. Considering the temperature factor for CO_2 adsorption at the Fe-O-Fe site, the Gibbs free energy (ΔG) of the reaction between CO_2 and SFMSc at different temperatures is given in Fig. S1. ΔG is shown to be greater than zero at roughly 450°C, implying that SFMSc could be stable against CO_2 at H-SOFC testing temperatures (600–700°C). Although ΔG is less than zero at tem-

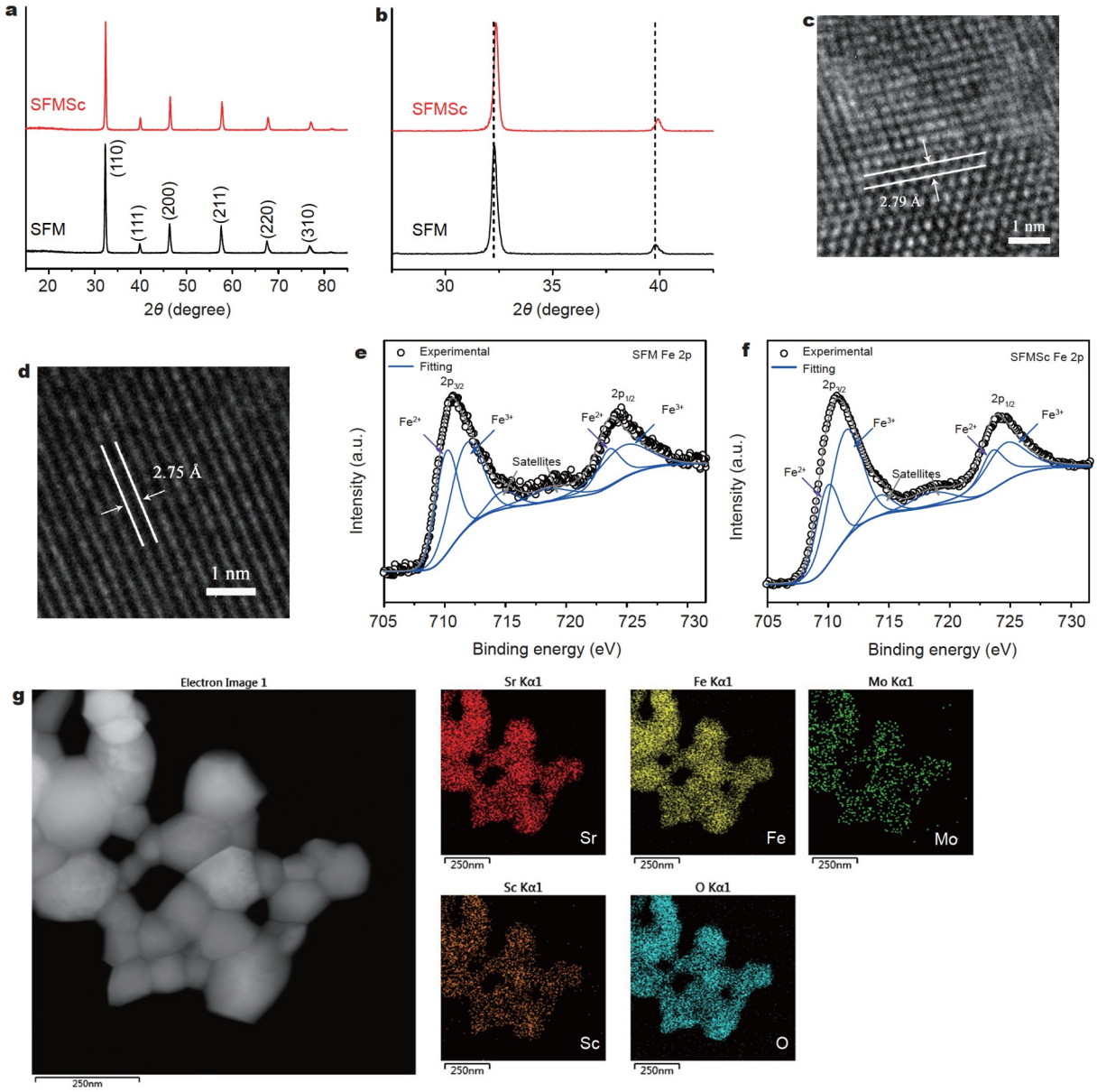

Figure 1 (a) XRD patterns and (b) enlarged XRD view of SFM and SFMSc powders; HRTEM images for (c) SFM and (d) SFMSc; XPS Fe 2p spectra for (e) SFM and (f) SFMSc; (g) STEM mapping for SFMSc.

peratures less than 400°C, no secondary phases were observed during the *in-situ* XRD test at these temperatures (Fig. 2b), implying that the possible reaction is kinetically very slow at these low temperatures and should not pose a significant problem for the stability of SMFSc as the cathode. Given that the CO_2 concentration in the stability test is 10%, and the CO_2 content in the air is only 0.03%, it is plausible to expect that SFMSc will be stable in these working conditions. To further investigate the chemical stability of SFMSc, harsh testing conditions with greater CO_2 concentration and longer testing time were applied. For 100 h, the SFMSc powder was treated at 700°C in 20% CO_2. The phase composition of the treated SFMSc detected by XRD (Fig. S2) demonstrates that there are no impurities after the treatment, confirming the excellent chemical stability of SFMSc against CO_2.

The DFT simulations are used to further investigate the suitability of SFMSc as a cathode for H-SOFCs. One reason for employing the Sc-doping technique is to generate more oxygen vacancies (Vo), which are critical for cathode performance. As a result, the Vo formation energy (E_{vo}) is computed and compared, revealing that the E_{vo} values for SFM and SFMSc are 1.01 and 0.67 eV, respectively. Although both values are greater than zero, the Sc-doped sample has a lower energy value, implying that the formation of Vo is more likely in SFMSc than in Sc-free SFM. The charge density difference results in Fig. 3a, b demonstrate that Sc doping may result in charge accumulation at neighboring oxygen atoms, weakening the metal–O bond and so favoring the formation of Vo [42]. The XPS study also demonstrated higher Vo content in SFMSc. The XPS O 1s spectra of SFM and SFMSc are shown in Fig. 3c, d, which can be fitted with four peaks: lattice O, O^-/O_2^{2-}, adsorbed surface OH^-/O_2, and surface H_2O. The oxygen vacancy concentration is

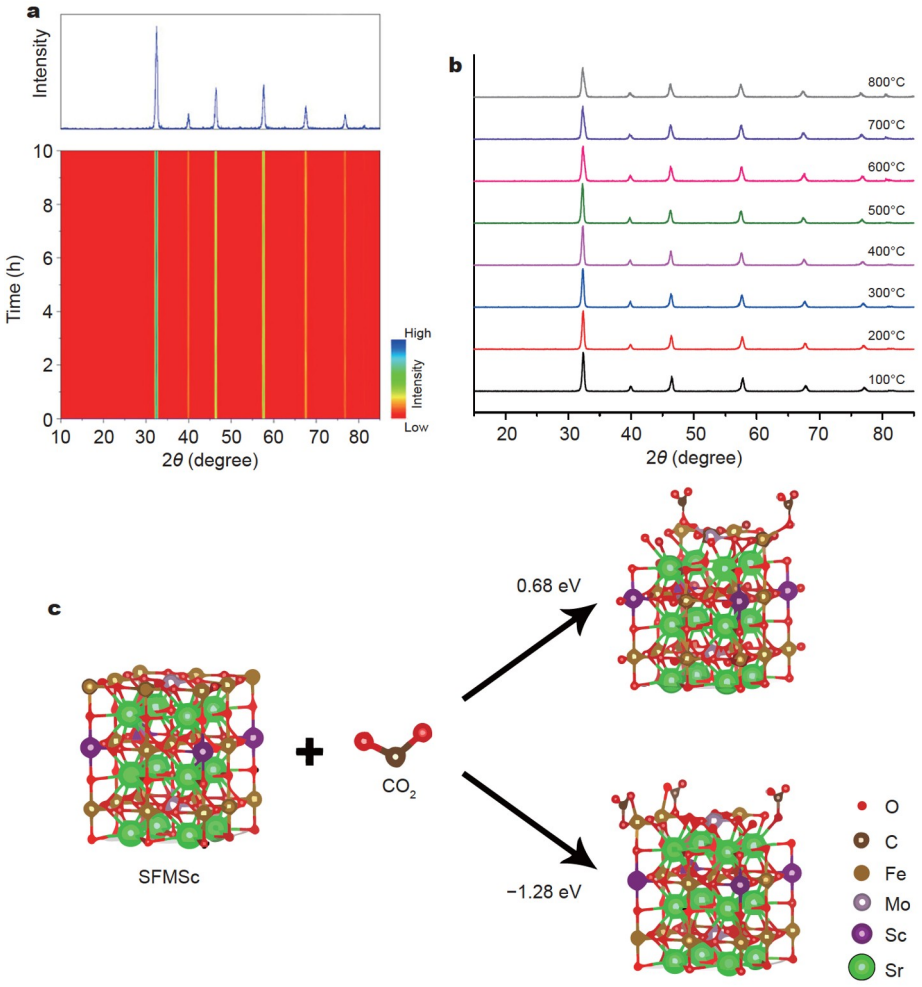

Figure 2 (a) Dynamic variation of the high-temperature XRD patterns for the SFMSc powder tested at 700°C in the CO_2-containing atmosphere. The XRD pattern for SFMSc powder after the CO_2 test is shown at the top; (b) *in-situ* XRD patterns for the SFMSc powder tested in the temperature range of 100–800°C in the CO_2-containing atmosphere; (c) the configuration and adsorption energy of CO_2 at the surface of SFMSc calculated by the DFT method.

reflected in the area ratio for the peaks corresponding to surface adsorbed OH^-/O_2 and lattice O [43–46]. The surface adsorbed OH^-/O_2 to lattice O ratio in SFM is 1.2, and it increases to 1.8 for SFMSc, which is consistent with the DFT calculation results and suggests that the addition of Sc into SFM favors the formation of oxygen vacancies.

Besides the formation of Vo, another critical parameter for proton-conducting oxides is protonation ability, often known as hydration [47–50]. Table 1 highlights and contrasts some major parameters estimated by the DFT approach for SFM and SFMSc. SFM and SFMSc have derived hydration energies (E_{hydra}) of −0.56 and −0.52 eV, respectively. Even though Sc doping marginally increases the energy value, the negative values of E_{hydra} indicate that the hydration procedure is thermodynamically favorable for both SFM and SFMSc. However, when proton transportations are considered, the Sc-doping technique has further advantages. The proton migrates in oxides *via* the oxygen atoms, and the rate-limiting step is the hopping step [50], as shown in Fig. 4a. The energy barrier for proton migration in SFM is 2.16 eV; however, it is lowered to 0.95 eV in Sc-doped SFM. It is obvious that doping Sc into SFM can lower the barrier for proton migration, hence facilitating proton transport in the oxide. The enhanced proton diffusion kinetics for SFMSc measured by ECR further demonstrates better proton migration capabilities. The conductivity of the sample would change due to the change of the charge carriers [48]. The time required to attain a new equilibrium in conductivity provides information on ion diffusions. Fig. 4b depicts the ECR curves for SFM and SFMSc tested at 600°C. By changing the gas from dry to wet air, the transition time for SFM is lowered to roughly 3000 s, while for SFMSc, the period is significantly reduced to around 600 s. The SFMSc response is substantially faster, implying that the diffusion of protons is faster in SFMSc than in SFM. The chemical diffusion coefficients for SFM and SFMSc were calculated to be 1.7×10^{-5} and 1.0×10^{-4} cm^2 s^{-1}, respectively, implying that the addition of Sc can improve proton diffusion, which is consistent with the DFT calculations.

The ORR activity of the material is another important parameter for cathodes since it indicates the cathode's catalytic activity toward O_2 [51]. Although SFMSc has a greater Vo content, implying that it may have superior ORR activity than SFM [46], DFT calculations can provide insights at the atomic level. There are two surface terminals, the Fe-Mo-O surface and the Fe-Sc-O surface, and it is discovered that the surface energy

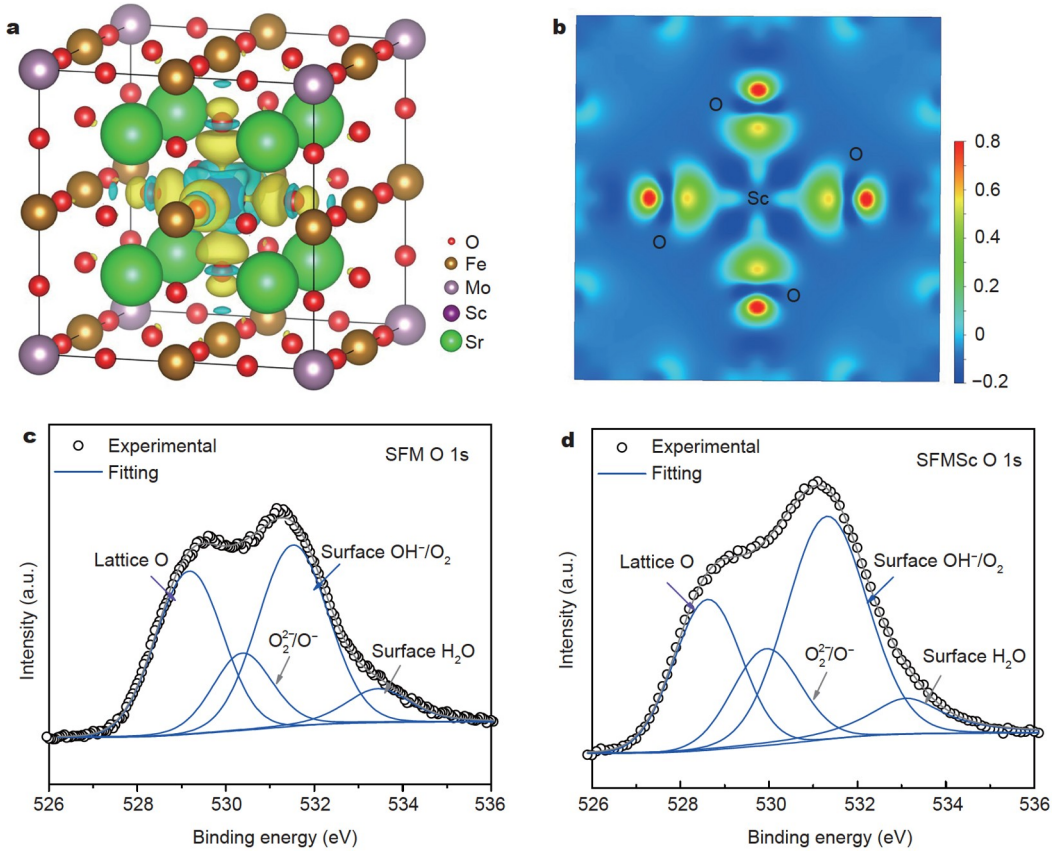

Figure 3 (a) Charge density difference for SFM with Sc-doping (yellow bubble: charge accumulation; blue bubble: charge depletion); (b) 2D contour plot corresponding to (a); O 1s binding energy curves for (c) SFM and (d) SFMSc.

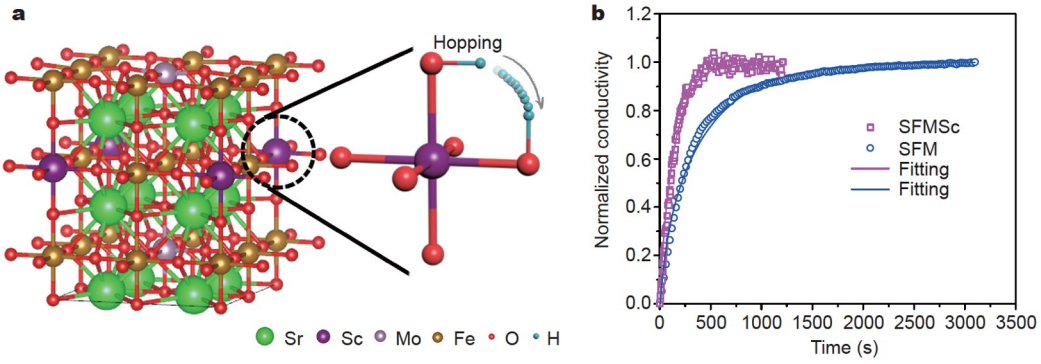

Figure 4 (a) Scheme for the proton hopping procedure; (b) ECR curves for SFM and SFMSc upon the change of the atmosphere from dry to wet (3% H_2O) air tested at 600°C.

of the Fe-Mo-O surface is lower than that of the Fe-Sc-O surface, implying that the Fe-Mo-O surface is more stable than the Fe-Sc-O surface from the DFT point of view [39]. As a result, the Fe-Mo-O surface is chosen for subsequent surface computations. Fig. 5 depicts two ORR processes: O_2 adsorption and dissociation. The O_2 adsorption energy on the SFM surface is −0.83 eV, indicating that O_2 adsorption is thermodynamically favorable at the SFM surface. When Sc is present in the materials, the value of O_2 adsorption energy rises to 0.05 eV, indicating that Sc doping raises the energy barrier for O_2 adsorption. Although the Sc-free SFM outperforms the Sc-containing SFM in the O_2 adsorption step, the opposite tendency is observed in the O_2 dissociation step. For dissociating O_2, SFM must overcome an energy barrier of 3.57 eV, which is substantially lower on the SFMSc surface at 0.89 eV. It is worth noting that the energy for

Table 1 Oxygen vacancy formation energy (E_{vo}), hydration energy (E_{hydra}), and proton migration energy barrier (E_m) for SFM and SFMSc calculated by the DFT method

	SFM	SFMSc
E_{vo} (eV)	1.01	0.67
E_{hydra} (eV)	−0.56	−0.52
E_m (eV)	2.16	0.95

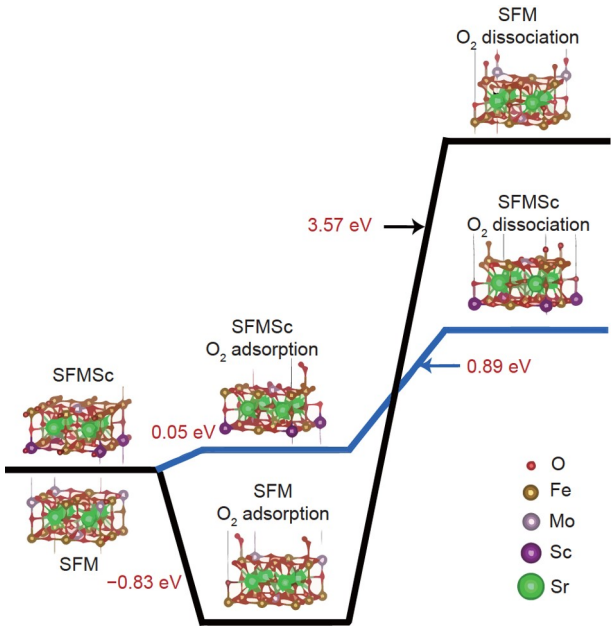

Figure 5 O_2 adsorption and dissociation procedure on SFM and SFMSc surfaces with the predicted energy barriers calculated from the DFT method.

O_2 dissociation is significantly higher than the energy for O_2 adsorption on both SFM and SFMSc. As a result, the rate-limiting step for the overall ORR is O_2 dissociation, resulting in a greater overall energy barrier in the ORR process for SFM without Sc addition.

The preceding experiments and DFT calculations show that doping Sc in SFM increases the formation of Vo and promotes proton migrations in the oxide, resulting in an improved surface ORR catalysis, implying that SFMSc has a high potential in H-SOFCs. As a result, the performance of the H-SOFC with the SFMSc cathode was evaluated and compared with that of the cell containing the Sc-free SFM cathode. Even though SFMSc was employed as a single-phase cathode without connecting the proton-conducting oxide to form the composites, the SFMSc cathode still makes contact with the BCZY electrolyte. As a result, the chemical compatibility of SFMSc and BCZY should be investigated. The XRD patterns for the SFMSc+BCZY composite powder before and after co-firing at the cathode/electrolyte co-sintering temperature (850°C) are shown in Fig. S3. After firing, no secondary phase was discovered in the composite powder, indicating high chemical compatibility between SFMSc and BCZY, and no newly formed phase could contribute to the electrochemical performance of the cells. Fig. 6a depicts the *I-V* and power density curves of cells using the SFMSc cathode at various temperatures. The SFMSc cell has peak power densities (PPDs) of 545, 966, and 1258 mW cm^{-2} at 600, 650, and 700°C, respectively. The performance is much higher than that of the SFM cell, with values of 368, 621, and 880 mW cm^{-2} at 600, 650, and 700°C, respectively (Fig. 6b). As shown in Fig. 6c, there has been a significant improvement in performance. Because both cells are fabricated in the same way except for the cathode, the cathode should play a dominating role in the variation in cell performance. After testing, the microstructure of the cells was examined using SEM. The morphologies of the SFMSc and SFM cells are depicted in Fig. 6d, e. Both cells have a tri-layer structure that consists of a Ni-BCZY anode, a BCZY electrolyte, and the SFMSc (or SFM) cathode. Furthermore, the SFMSc and SFM cathodes have similar morphology, implying that the differences in cell performance are not attributable to microstructure concerns but rather to the increased catalytic properties of the SFM cathode with Sc-doping. Fig. 7a, b depict the proposed reaction mechanism. At the SFM/BCZY electrolyte contact, the active reaction region, known as triple phase boundaries, is constrained. The SFMSc cathode, on the other hand, has a significantly larger area that extends to the overall cathode surface due to the introduction of protonation in this material. Furthermore, the improved ORR activity of SFMSc allows for faster ORR at the SFMSc surface, which accelerates the overall fuel cell reaction $2H_2 + O_2 \rightarrow 2H_2O$. The improved catalytic activity of SFMSc is also demonstrated with the electrochemical impedance spectroscopy (EIS) measurements, as illustrated in Fig. 7c. The polarization resistance (R_p) of the SFMSc cell is 0.043 Ω cm^2, which is significantly lower than that of the SFM cell, which is 0.084 Ω cm^2, indicating that the SMFSc's high catalytic activity allows for a faster reaction over the cathode, resulting in lower R_p and improved fuel cell performance. Aside from increased cell performance, the SFMSc cell exhibits good operational stability, running continuously for more than 200 h, as illustrated in Fig. 7d.

In addition to higher fuel cell performance and lower R_p for the SFMSc cathode compared with the Sc-free cathode, the current SFMSc cell outperforms most H-SOFCs using single-phase cathodes [52–55]. It should be noted that the current cell employs a single-phase SFMSc cathode without coupling the electrolyte material in the cathode. Even in this scenario, the performance is superior to that of several H-SOFCs with composite cathodes [41,56–59]. In the case of conventional H-SOFC cathodes, proton-conducting electrolyte materials are usually mixed with the cathode material to form the cathode composite, thereby extending the active reaction area to the two-phase connections [25]. The proton conduction in this design is accomplished through the proton-conducting phase in the composite cathodes. In comparison, the single-phase cathode would extend the reaction area to the entire cathode area, assuming the single-phase cathode has sufficient proton diffusion ability. Several high-performance single-phase cathodes have been proposed in recent years [20,60,61], and these cathodes greatly improve cell performance. However, due to the high catalytic activity of cobalt-based oxides, most of these high-performance single-phase cathodes must employ cobalt as one of the major components. As a result, developing a cobalt-free single-phase cathode with high performance for H-SOFCs remains a challenge. Table 2 highlights the performance of cobalt-free single-phase cathode H-SOFCs reported in the literature [36,52,53,62–67]. One can see that the attempt to use single-phase cathodes without cobalt was made more than ten years ago but with no satisfactory performance at the time. Efforts over the last decade have improved performance through the redesign of the cathode composition, the modification of nanoparticles, and the optimization of the microstructure (such as the use of nanofiber). Even when compared with these techniques, the SFMSc cathode revealed in this study outperforms most cobalt-free single-phase cathodes previously reported, yielding superior fuel cell performance and lower R_p, as shown in Table 2. To the best of our knowledge, only the Sn and Bi co-doped $BaFeO_3$ (BSFB) cathode with the proper amount of Sn reported by Xia *et al.* [65] allows a slightly higher perfor-

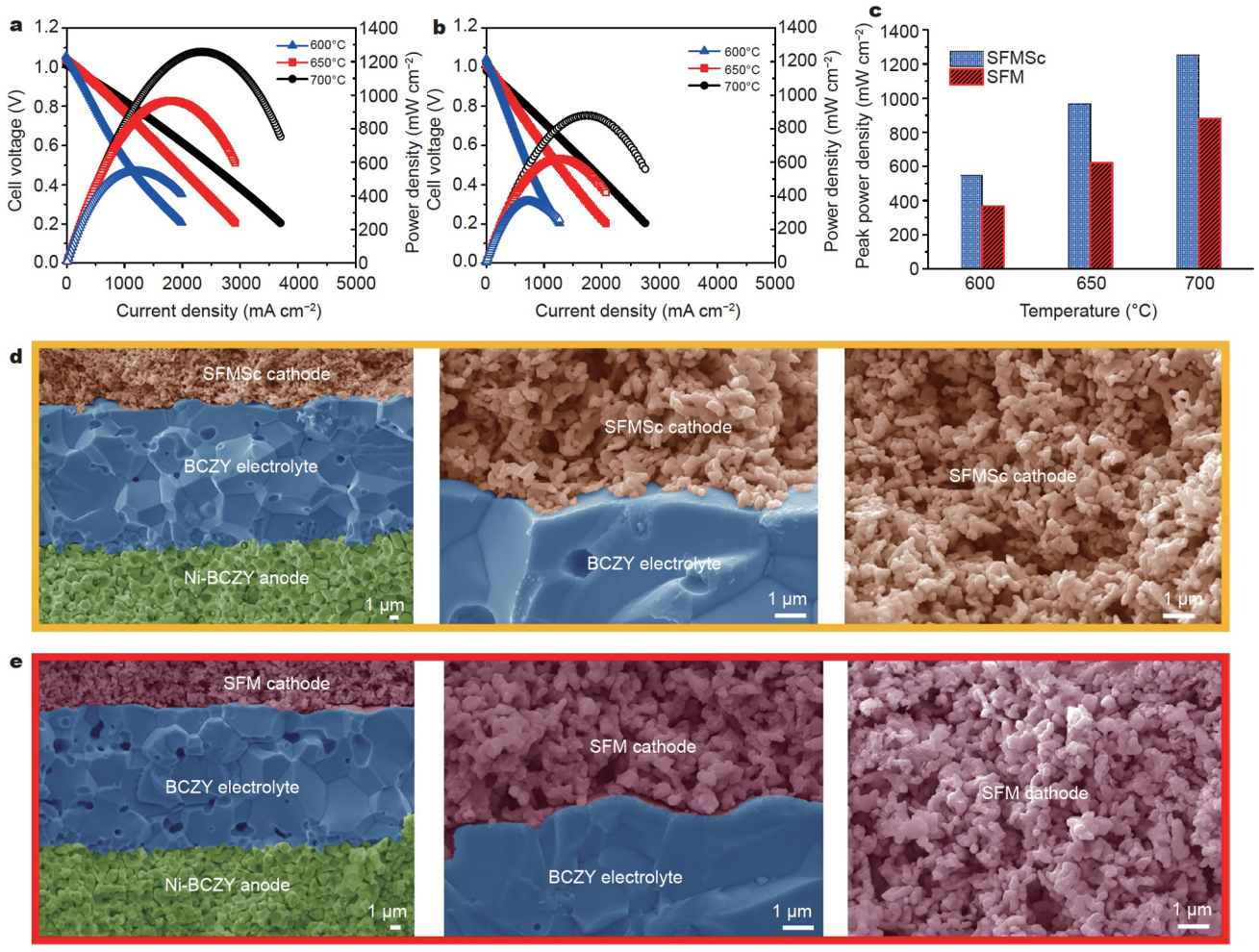

Figure 6 *I-V* and power density curves for (a) SFMSc and (b) SFM cell; (c) the PPD comparison between SFM and SFMSc cells at different temperatures; the cross-sectional views for (d) SFM and (e) SFMSc cells.

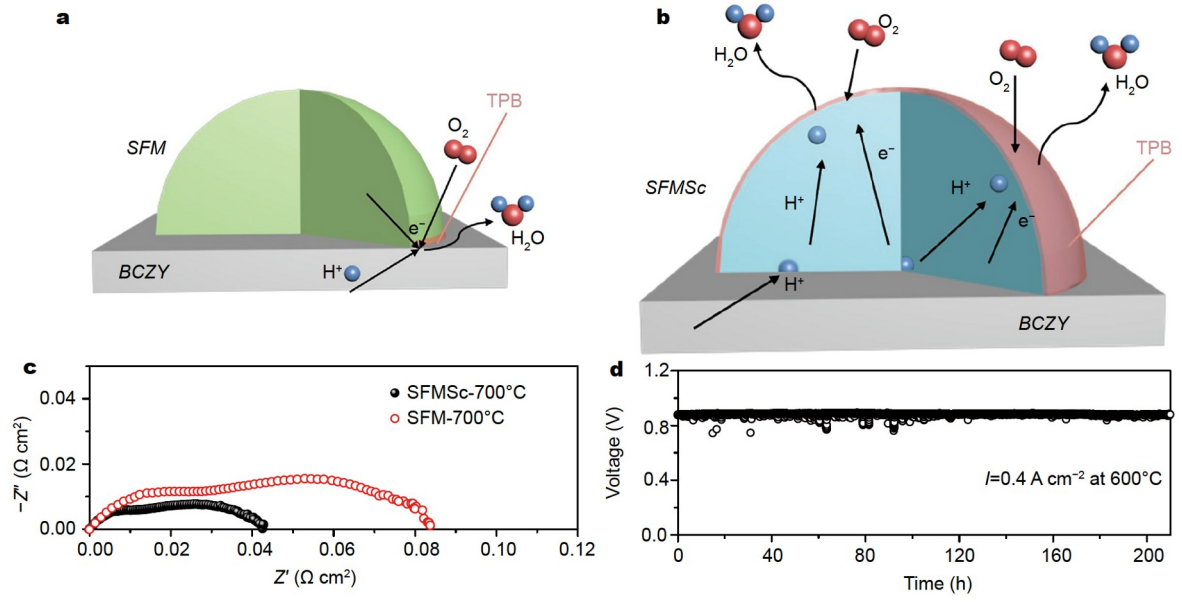

Figure 7 Schemes for cathode reactions on (a) SFM and (b) SFMSc; (c) EIS plots for the SFM and SFMSc cells tested at 700°C; (d) long-term stability test for the SFMSc cell operated at 600°C under a constant current density of 0.4 A cm^{-2}.

Table 2 Performance comparison of H-SOFCs using cobalt-free single-phase cathodes reported in the literature and the present study. The performances of these cells were measured at 700°C.

Year (Reference)	Cathode	PPD (mW cm^{-2})	R_p (Ω cm^2)
2009 (Ref. 52)	$BaCe_{0.5}Bi_{0.5}O_{3-\delta}$	321	0.28
2009 (Ref. 53)	$BaCe_{0.5}Fe_{0.5}O_{3-\delta}$	395	0.17
2015 (Ref. 62)	$Sr_3Fe_2O_{7-\delta}$	683	0.18
2018 (Ref. 63)	$La_{1.2}Sr_{0.8}NiO_{4+\delta}$	460	0.28
2018 (Ref. 63)	$Pr_{1.2}Sr_{0.8}NiO_{4+\delta}$	350	0.39
2019 (Ref. 64)	$La_2NiO_{4+\delta}$ (nanofiber)	508	0.17
2019 (Ref. 64)	$LaNi_{0.6}Fe_{0.4}O_{3-\delta}$ (nanofiber)	551	0.13
2019 (Ref. 65)	$BaFe_{0.5}Sn_{0.2}Bi_{0.3}O_{3-\delta}$	1277	0.032
2019 (Ref. 66)	$La_{1.2}Sr_{0.8}Ni_{0.6}Fe_{0.4}O_{4+\delta}$	781	0.078
2020 (Ref. 36)	$Sr_2Fe_{1.5}Mo_{0.4}Zr_{0.1}O_{6-\delta}$	790	0.11
2020 (Ref. 67)	$Pr_2BaNiMnO_{7-\delta}$	1070	0.084
This study	SFMSc	1258	0.043

mance than the SFMSc cell. The high basicity of the Ba-element may boost the hydration ability of the BSFB material, allowing it to exhibit promising electrochemical properties for H-SOFCs even without cobalt. However, the high Ba-concentration in proton-conducting oxides usually has a negative impact on chemical stability [68], making it difficult to find a balance between electrochemical performance and chemical stability. There is no Ba-element in the composition of the SFMSc cathode employed in this study, and its high chemical stability has already been demonstrated, as indicated above. As a result, the SFMSc cathode integrates high electrochemical performance with outstanding chemical stability, providing a new path for cathode design.

CONCLUSIONS

High-performance cathode materials with good catalytic activity and high proton diffusivity are highly desired for H-SOFCs, motivating researchers to synthesize a new cathode by modifying the conventional SFM with Sc ions. From atomic level computations, the SFMSc is predicted to have lower Vo formation energy and lower energy barriers in proton migration, as well as better ORR activity. The theoretical calculation results supported by experimental studies demonstrate that the SFMSc cathode has a higher proton diffusion rate and a lower polarization resistance than the Sc-free cathode. As a result, the SFMSc cell outperforms the SFM cell significantly. Although SFMSc is utilized as a single-phase cathode in H-SOFCs, its performance is superior to that of many H-SOFCs that employ composite cathodes (that is, coupling the cathode and electrolyte materials to extend the active reaction zone). When compared with other cobalt-free single-phase cathodes for H-SOFCs, the current SFMSc cathode exhibits one of the best performances ever reported. The exceptional chemical stability of SFMSc does not compromise its good electrochemical performance, indicating a high potential for SFMSc in H-SOFCs.

Received 25 October 2021; accepted 14 December 2021; published online 18 February 2022

1 Zhang Y, Chen B, Guan D, *et al.* Thermal-expansion offset for high-performance fuel cell cathodes. Nature, 2021, 591: 246–251
2 Wachsman E, Ishihara T, Kilner J. Low-temperature solid-oxide fuel cells. MRS Bull, 2014, 39: 773–779
3 Chen K, Jiang SP. Surface segregation in solid oxide cell oxygen electrodes: Phenomena, mitigation strategies and electrochemical properties. Electrochem Energ Rev, 2020, 3: 730–765
4 Kilner JA, Burriel M. Materials for intermediate-temperature solid-oxide fuel cells. Annu Rev Mater Res, 2014, 44: 365–393
5 Li P, Yang W, Tian C, *et al.* Electrochemical performance of $La_2NiO_{4+\delta}$-$Ce_{0.55}La_{0.45}O_{2-\delta}$ as a promising bifunctional oxygen electrode for reversible solid oxide cells. J Adv Ceram, 2021, 10: 328–337
6 Wang W, Tian Y, Liu Y, *et al.* Tailored Sr-Co-free perovskite oxide as an air electrode for high-performance reversible solid oxide cells. Sci China Mater, 2021, 64: 1621–1631
7 Li Y, Singh M, Zhuang Z, *et al.* Efficient reversible CO/CO_2 conversion in solid oxide cells with a phase-transformed fuel electrode. Sci China Mater, 2021, 64: 1114–1126
8 Chen M, Chen D, Wang K, *et al.* Densification and electrical conducting behavior of $BaZr_{0.9}Y_{0.1}O_{3-\delta}$ proton conducting ceramics with NiO additive. J Alloys Compd, 2019, 781: 857–865
9 Medvedev D, Murashkina A, Pikalova E, *et al.* $BaCeO_3$: Materials development, properties and application. Prog Mater Sci, 2014, 60: 72–129
10 Li J, Wang C, Wang X, *et al.* Sintering aids for proton-conducting oxides—A double-edged sword? A mini review. Electrochem Commun, 2020, 112: 106672
11 Dai H, Kou H, Wang H, *et al.* Electrochemical performance of protonic ceramic fuel cells with stable bazro3-based electrolyte: A mini-review. Electrochem Commun, 2018, 96: 11–15
12 Tarutin AP, Lyagaeva JG, Medvedev DA, *et al.* Recent advances in layered $Ln_2NiO_{4+\delta}$ nickelates: fundamentals and prospects of their applications in protonic ceramic fuel and electrolysis cells. J Mater Chem A, 2021, 9: 154–195
13 Chen M, Xie X, Guo J, *et al.* Space charge layer effect at the platinum anode/$BaZr_{0.9}Y_{0.1}O_{3-\delta}$ electrolyte interface in proton ceramic fuel cells. J Mater Chem A, 2020, 8: 12566–12575
14 Bi L, Boulfrad S, Traversa E. Steam electrolysis by solid oxide electrolysis cells (SOECs) with proton-conducting oxides. Chem Soc Rev, 2014, 43: 8255–8270
15 Fabbri E, Bi L, Pergolesi D, *et al.* Towards the next generation of solid oxide fuel cells operating below 600°C with chemically stable proton-conducting electrolytes. Adv Mater, 2012, 24: 195–208
16 Peng R, Wu T, Liu W, *et al.* Cathode processes and materials for solid oxide fuel cells with proton conductors as electrolytes. J Mater Chem, 2010, 20: 6218–6225
17 Lin Y, Ran R, Zhang C, *et al.* Performance of $PrBaCo_2O_{5+\delta}$ as a proton-conducting solid-oxide fuel cell cathode. J Phys Chem A, 2010, 114: 3764–3772
18 Guo Y, Lin Y, Ran R, *et al.* Zirconium doping effect on the performance of proton-conducting $BaZr_yCe_{0.8-y}Y_{0.2}O_{3-\delta}$ ($0.0\leq y\leq 0.8$) for fuel cell applications. J Power Sources, 2009, 193: 400–407

19 Kim J, Sengodan S, Kwon G, *et al.* Triple-conducting layered perovskites as cathode materials for proton-conducting solid oxide fuel cells. ChemSusChem, 2014, 7: 2811–2815
20 Choi S, Kucharczyk CJ, Liang Y, *et al.* Exceptional power density and stability at intermediate temperatures in protonic ceramic fuel cells. Nat Energy, 2018, 3: 202–210
21 Xu X, Xu Y, Ma J, *et al.* Tailoring electronic structure of perovskite cathode for proton-conducting solid oxide fuel cells with high performance. J Power Sources, 2021, 489: 229486
22 Wang N, Hinokuma S, Ina T, *et al.* Mixed proton–electron–oxide ion triple conducting manganite as an efficient cobalt-free cathode for protonic ceramic fuel cells. J Mater Chem A, 2020, 8: 11043–11055
23 Zhou C, Sunarso J, Song Y, *et al.* New reduced-temperature ceramic fuel cells with dual-ion conducting electrolyte and triple-conducting double perovskite cathode. J Mater Chem A, 2019, 7: 13265–13274
24 Xu X, Wang H, Fronzi M, *et al.* Tailoring cations in a perovskite cathode for proton-conducting solid oxide fuel cells with high performance. J Mater Chem A, 2019, 7: 20624–20632
25 Fabbri E, Pergolesi D, Traversa E. Materials challenges toward proton-conducting oxide fuel cells: A critical review. Chem Soc Rev, 2010, 39: 4355–4369
26 Bi L, Shafi SP, Da'as EH, *et al.* Tailoring the cathode-electrolyte interface with nanoparticles for boosting the solid oxide fuel cell performance of chemically stable proton-conducting electrolytes. Small, 2018, 14: 1801231
27 Song Y, Chen Y, Wang W, *et al.* Self-assembled triple-conducting nanocomposite as a superior protonic ceramic fuel cell cathode. Joule, 2019, 3: 2842–2853
28 Tong X, Xu Y, Tripković Đ, *et al.* Promotion of oxygen reduction and evolution by applying a nanoengineered hybrid catalyst on cobalt free electrodes for solid oxide cells. J Mater Chem A, 2020, 8: 9039–9048
29 Yuan R, He W, Zhang C, *et al.* Cobalt free $SrFe_{0.95}Nb_{0.05}O_{3-\delta}$ cathode material for proton-conducting solid oxide fuel cells with $BaZr_{0.1}Ce_{0.7}Y_{0.2}O_{3-\delta}$ electrolyte. Mater Lett, 2017, 200: 75–78
30 Muñoz-García AB, Pavone M, Ritzmann AM, *et al.* Oxide ion transport in $Sr_2Fe_{1.5}Mo_{0.5}O_{6-\delta}$, a mixed ion-electron conductor: new insights from first principles modeling. Phys Chem Chem Phys, 2013, 15: 6250–6259
31 Liu Q, Bugaris DE, Xiao G, *et al.* $Sr_2Fe_{1.5}Mo_{0.5}O_{6-\delta}$ as a regenerative anode for solid oxide fuel cells. J Power Sources, 2011, 196: 9148–9153
32 Meng X, Wang Y, Zhao Y, *et al. In-situ* exsolution of nanoparticles from Ni substituted $Sr_2Fe_{1.5}Mo_{0.5}O_6$ perovskite oxides with different Ni doping contents. Electrochim Acta, 2020, 348: 136351
33 Yang Y, Wang Y, Yang Z, *et al.* Co-substituted $Sr_2Fe_{1.5}Mo_{0.5}O_{6-\delta}$ as anode materials for solid oxide fuel cells: Achieving high performance via nanoparticle exsolution. J Power Sources, 2019, 438: 226989
34 Xu C, Zhen S, Ren R, *et al.* Cu-doped $Sr_2Fe_{1.5}Mo_{0.5}O_{6-\delta}$ as a highly active cathode for solid oxide electrolytic cells. Chem Commun, 2019, 55: 8009–8012
35 Qiu P, Lin J, Lei L, *et al.* Evaluation of Cr-tolerance of the $Sr_2Fe_{1.5}Mo_{0.5}O_{6-\delta}$ cathode for solid oxide fuel cells. ACS Appl Energy Mater, 2019, 2: 7619–7627
36 Ren R, Wang Z, Meng X, *et al.* Tailoring the oxygen vacancy to achieve fast intrinsic proton transport in a perovskite cathode for protonic ceramic fuel cells. ACS Appl Energy Mater, 2020, 3: 4914–4922
37 Da'as EH, Bi L, Boulfrad S, *et al.* Nanostructuring the electronic conducting $La_{0.8}Sr_{0.2}MnO_{3-\delta}$ cathode for high-performance in proton-conducting solid oxide fuel cells below 600°C. Sci China Mater, 2018, 61: 57–64
38 Kresse G, Furthmüller J. Efficient iterative schemes for *ab initio* total-energy calculations using a plane-wave basis set. Phys Rev B, 1996, 54: 11169–11186
39 Muñoz-García AB, Tuccillo M, Pavone M. Computational design of cobalt-free mixed proton–electron conductors for solid oxide electrochemical cells. J Mater Chem A, 2017, 5: 11825–11833
40 Henkelman G, Uberuaga BP, Jónsson H. A climbing image nudged elastic band method for finding saddle points and minimum energy paths. J Chem Phys, 2000, 113: 9901–9904
41 Liu W, Kou H, Wang X, *et al.* Improving the performance of the $Ba_{0.5}Sr_{0.5}Co_{0.8}Fe_{0.2}O_3$ cathode for proton-conducting SOFCs by microwave sintering. Ceramics Int, 2019, 45: 20994–20998
42 Lu X, Yang X, Jia L, *et al.* First principles study on the oxygen reduction reaction of the $La_{1-x}Sr_xMnO_3$ coated $Ba_{1-x}Sr_xCo_{1-y}Fe_yO_3$ cathode for solid oxide fuel cells. Int J Hydrogen Energy, 2019, 44: 16359–16367
43 Zhang X, Pei C, Chang X, *et al.* FeO_6 octahedral distortion activates lattice oxygen in perovskite ferrite for methane partial oxidation coupled with CO_2 splitting. J Am Chem Soc, 2020, 142: 11540–11549
44 Xu Y, Xu X, Cao N, *et al.* Perovskite ceramic oxide as an efficient electrocatalyst for nitrogen fixation. Int J Hydrogen Energy, 2021, 46: 10293–10302
45 Xu Y, Liu X, Cao N, *et al.* Defect engineering for electrocatalytic nitrogen reduction reaction at ambient conditions. Sustain Mater Technologies, 2021, 27: e00229
46 Ji Q, Xu X, Liu X, *et al.* Improvement of the catalytic properties of porous lanthanum manganite for the oxygen reduction reaction by partial substitution of strontium for lanthanum. Electrochem Commun, 2021, 124: 106964
47 Wu S, Xu X, Li X, *et al.* High-performance proton-conducting solid oxide fuel cells using the first-generation Sr-doped $LaMnO_3$ cathode tailored with Zn ions. Sci China Mater, 2022, 65: 675–682
48 Han D, Uemura S, Hiraiwa C, *et al.* Detrimental effect of sintering additives on conducting ceramics: yttrium-doped barium zirconate. ChemSusChem, 2018, 11: 4102–4113
49 Tao Z, Xu X, Bi L. Density functional theory calculations for cathode materials of proton-conducting solid oxide fuel cells: A mini-review. Electrochem Commun, 2021, 129: 107072
50 Kreuer KD. Proton-conducting oxides. Annu Rev Mater Res, 2003, 33: 333–359
51 Ji Q, Bi L, Zhang J, *et al.* The role of oxygen vacancies of ABO_3 perovskite oxides in the oxygen reduction reaction. Energy Environ Sci, 2020, 13: 1408–1428
52 Tao Z, Bi L, Yan L, *et al.* A novel single phase cathode material for a proton-conducting SOFC. Electrochem Commun, 2009, 11: 688–690
53 Tao Z, Bi L, Zhu Z, *et al.* Novel cobalt-free cathode materials $BaCe_xFe_{1-x}O_{3-\delta}$ for proton-conducting solid oxide fuel cells. J Power Sources, 2009, 194: 801–804
54 Rao Y, Zhong S, He F, *et al.* Cobalt-doped $BaZrO_3$: A single phase air electrode material for reversible solid oxide cells. Int J Hydrogen Energy, 2012, 37: 12522–12527
55 Zhang Y, Zhu A, Guo Y, *et al.* Electrochemical performance and effect of moisture on $Ba_{0.5}Sr_{0.5}Sc_{0.175}Nb_{0.025}Co_{0.8}O_{3-\delta}$ oxide as a promising electrode for proton-conducting solid oxide fuel cells. Appl Energy, 2019, 238: 344–350
56 Zhang Z, Wang J, Chen Y, *et al. In situ* formation of a 3D core-shell and triple-conducting oxygen reduction reaction electrode for proton-conducting SOFCs. J Power Sources, 2018, 385: 76–83
57 Shao L, Si F, Fu XZ, *et al.* Stable $SrCo_{0.7}Fe_{0.2}Zr_{0.1}O_{3-\delta}$ cathode material for proton conducting solid oxide fuel cell reactors. Int J Hydrogen Energy, 2018, 43: 7511–7514
58 Ma J, Tao Z, Kou H, *et al.* Evaluating the effect of Pr-doping on the performance of strontium-doped lanthanum ferrite cathodes for protonic SOFCs. Ceramics Int, 2020, 46: 4000–4005
59 He B, Zhang L, Zhang Y, *et al.* New insight into highly active cathode of proton conducting solid oxide fuel cells by oxygen ionic conductor modification. J Power Sources, 2015, 287: 170–176
60 Bae K, Jang DY, Choi HJ, *et al.* Demonstrating the potential of yttrium-doped barium zirconate electrolyte for high-performance fuel cells. Nat Commun, 2017, 8: 14553
61 Duan C, Tong J, Shang M, *et al.* Readily processed protonic ceramic fuel cells with high performance at low temperatures. Science, 2015, 349: 1321–1326
62 Wang Z, Yang W, Shafi SP, *et al.* A high performance cathode for proton conducting solid oxide fuel cells. J Mater Chem A, 2015, 3: 8405–8412
63 Yang S, Wen Y, Zhang J, *et al.* Electrochemical performance and stability of cobalt-free $Ln_{1.2}Sr_{0.8}NiO_4$ (Ln=La and Pr) air electrodes for proton-conducting reversible solid oxide cells. Electrochim Acta, 2018, 267: 269–277
64 Tang H, Jin Z, Wu Y, *et al.* Cobalt-free nanofiber cathodes for proton

conducting solid oxide fuel cells. Electrochem Commun, 2019, 100: 108–112
65 Xia Y, Jin Z, Wang H, *et al.* A novel cobalt-free cathode with triple-conduction for proton-conducting solid oxide fuel cells with unprecedented performance. J Mater Chem A, 2019, 7: 16136–16148
66 Miao L, Hou J, Gong Z, *et al.* A high-performance cobalt-free Ruddlesden-Popper phase cathode $La_{1.2}Sr_{0.8}Ni_{0.6}Fe_{0.4}O_{4+\delta}$ for low temperature proton-conducting solid oxide fuel cells. Int J Hydrogen Energy, 2019, 44: 7531–7537
67 Wang Q, Hou J, Fan Y, *et al.* $Pr_2BaNiMnO_{7-\delta}$ double-layered Ruddlesden–Popper perovskite oxides as efficient cathode electrocatalysts for low temperature proton conducting solid oxide fuel cells. J Mater Chem A, 2020, 8: 7704–7712
68 Matsumoto H, Sakai T, Okuyama Y. Proton-conducting oxide and applications to hydrogen energy devices. Pure Appl Chem, 2013, 85: 427–435

Acknowledgements This work was supported by the National Natural Science Foundation of China (51972183) and the Startup Funding for Talents at the University of South China.

Author contributions Zhang L, Yin Y, and Bi L designed the study and analyzed the data. Zhang L, Yin Y, Xu Y, and Yu S performed the experiments. Bi L wrote the manuscript with other co-authors, and all authors discussed the results and provided their approval to the final version.

Conflict of interest The authors declare that they have no conflict of interest.

Supplementary information Supporting data are available in the online version of the paper.

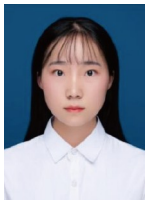

Liling Zhang is a postgraduate student in Prof. Lei Bi's group at the University of South China. Her research interests focus mostly on the development of new cathode materials for H-SOFCs and the exploration of the influence of microwave sintering on the characteristics of materials and the performance of H-SOFCs.

Yanru Yin was a research assistant in Prof. Lei Bi's group at the University of South China after she received her master's degree from Qingdao University. Her research interest is in tailoring the structure and properties of proton-conducting oxides, with the goal of understanding the charge carrier transport mechanism in proton-conducting oxides and then improving the performance of H-SOFCs.

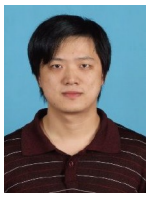

Lei Bi is a full professor at the University of South China and leads a research group that studies H-SOFCs utilizing both first-principles calculations and experimental methodologies. His research interests include the development and optimization of essential materials for H-SOFCs, as well as innovative fuel cell fabrication technologies. Another area of study that he is interested in is the development of new sintering processes for H-SOFC fabrication.

Sc掺杂的$Sr_2Fe_{1.5}Mo_{0.5}O_{6-\delta}$作为质子导体固体氧化物燃料电池的新型单相阴极

张醴陵[†], 尹燕儒[†], 许阳森, 于守富, 毕磊[*]

摘要 本文利用Sc元素部分取代 $Sr_2Fe_{1.5}Mo_{0.5}O_{6-\delta}$ (SFM) 中的Mo, 成功制备了具有高质子扩散速率的新型Sc掺杂SFM (SFMSc)材料. 理论计算表明, 将Sc掺杂到SFM中可以降低材料的氧空位形成能, 降低氧化物中质子迁移的能垒, 并提高材料氧还原反应的催化活性. 使用单相 SFMSc阴极的质子导体固体氧化物燃料电池 (H-SOFC)比使用不含Sc的SFM单相阴极电池具有更高的电池性能, 其在700°C时的性能达到1258 mW cm^{-2}. 该性能也超过了许多其他使用单相无钴阴极的H-SOFC. 此外, 材料良好的电化学性能并没有以牺牲其稳定性为代价. SFMSc材料在含 CO_2的气氛中以及在燃料电池工作条件下都表现出良好的稳定性. 高输出性能和良好的稳定性, 使SFMSc成为一种有潜力的高效的H-SOFC阴极材料.

